



**HAL**  
open science

## Adhesion of tungsten particles on rough tungsten surfaces using Atomic Force Microscopy

Samuel Peillon, Adrien Autricque, Michaël Redolfi, Cristian Stancu, François Gensdarmes, Christian Grisolia, Olivier Pluchery

► **To cite this version:**

Samuel Peillon, Adrien Autricque, Michaël Redolfi, Cristian Stancu, François Gensdarmes, et al.. Adhesion of tungsten particles on rough tungsten surfaces using Atomic Force Microscopy. *Journal of Aerosol Science*, 2019, 137, pp.105431. 10.1016/j.jaerosci.2019.105431 . hal-02322543

**HAL Id: hal-02322543**

<https://hal.sorbonne-universite.fr/hal-02322543v1>

Submitted on 21 Oct 2019

**HAL** is a multi-disciplinary open access archive for the deposit and dissemination of scientific research documents, whether they are published or not. The documents may come from teaching and research institutions in France or abroad, or from public or private research centers.

L'archive ouverte pluridisciplinaire **HAL**, est destinée au dépôt et à la diffusion de documents scientifiques de niveau recherche, publiés ou non, émanant des établissements d'enseignement et de recherche français ou étrangers, des laboratoires publics ou privés.

# Adhesion of tungsten particles on rough tungsten surfaces using Atomic Force Microscopy

Samuel Peillon<sup>a,e</sup>, Adrien Autricque<sup>b</sup>, Michaël Redolfi<sup>c</sup>, Cristian Stancu<sup>d</sup>, François Gensdarmes<sup>a</sup>, Christian Grisolia<sup>b</sup>, Olivier Pluchery<sup>e</sup>

<sup>a</sup>Institut de Radioprotection et de Sûreté Nucléaire (IRSN), PSN-RES/SCA, BP 68, 91192 Gif-sur-Yvette, France

<sup>b</sup>CEA, IRFM, F-13108 Saint Paul lez Durance, France

<sup>c</sup>LSPM, CNRS-UPR3407, Université Paris 13 Sorbonne Paris Cité, 99 Avenue J. B. Clément, 93430 Villetaneuse, France

<sup>d</sup>National Institute for Lasers, Plasma and Radiation Physics, Magurele, 077125, Romania

<sup>e</sup>Sorbonne Universités, UPMC-CNRS, Institut des Nanosciences de Paris, 4 place Jussieu, 75252 Paris, Cedex 05, France

---

## Abstract

Adhesion forces between tungsten spherical microparticles and tungsten substrates with different roughnesses have been measured using the Atomic Force Microscopy (AFM) colloidal probe technique. Mean roughnesses of the tungsten substrates were measured by AFM and were ranked in three categories i.e. nanoscale, sub-microscale and microscale roughnesses. Experimental Hamaker constant of  $37 \pm 3.5 \times 10^{-20}$  J has been obtained using a spherical tungsten particle of  $10.5 \mu\text{m}$  in radius and a tungsten substrate with nanoscale root-mean-square roughness of  $rms = 11.5$  nm. It was shown that larger roughness of the order  $rms = 712$  nm induces a two order of magnitude decrease on the adhesion of tungsten microparticles compared to a smooth tungsten surface with nanoscale roughness. Comparison with the van der Waals-based adhesion force model of Rabinovich which integrates the roughness of surfaces showed good agreement with experimental pull-off forces even when roughness of the substrate is close to the micrometer range. In such case, measurements have shown that dependency of adhesion force with particle size (in the micrometer range) has a secondary influence compared to the roughness of surfaces.

**Keywords:** Adhesion, Roughness, Tungsten, Hamaker constant, Atomic Force Microscopy

---

## 1 Introduction

2 The study of adhesion of microparticles on surfaces have numerous applications in many different fields of re-  
3 search. It is, for example, particularly of great importance in the evaluation of resuspension or removal of particu-  
4 late contaminants from rough surfaces encountered in domains such as biotechnology, micro and nanoelectronic or  
5 powder handling in pharmaceutical or nuclear industry. In this latter domain, special attention to the safety and oper-  
6 ation of next-generation nuclear fusion facilities has emerged over the years. Indeed, large amount of metallic dusts  
7 ([Krasheninnikov et al. \[2011\]](#)) will be generated by energetic plasma-surface interactions that cause significant erosion  
8 of the vacuum vessel (VV) plasma facing-components (PFCs) made from beryllium and tungsten. Characterization

---

Email address: [samuel.peillon@irsn.fr](mailto:samuel.peillon@irsn.fr) (Samuel Peillon)

9 of the behavior of these dusts and especially the amount of particles that can be re-suspended or are already airborne  
10 during normal operations is of primary interest for the design and the definition of the functioning procedure and  
11 safety domain of these facilities. Therefore, it is necessary to know *a priori* the adhesive properties of these particles  
12 on specific surfaces of interest such as rough tungsten or beryllium to evaluate their re-suspension potential. Despite  
13 its importance, the phenomenon of adhesion of particles on rough surfaces is difficult to measure in a quantitative way  
14 because of its complexity. For example, environmental conditions (humidity, temperature), geometry (size, rough-  
15 ness) of the surfaces in contact, energetic heterogeneity and chemical interactions can influence the adhesion force.  
16 In particular, value of adhesion energy for tungsten surfaces is still poorly documented and recent studies ([Rondeau  
17 et al. \[2015\]](#), [Peillon et al. \[2017\]](#), [Tolias et al. \[2018\]](#)) are questioning data found in the literature for this material.  
18 Detachment of microparticles from rough substrates is a process resulting from the competition between the removal  
19 force e.g. aerodynamic, electrostatic, centrifuge or inertial and the particle-surface interactions among them adhesive  
20 forces. In the case where a large number of microparticles are dispersed on a surface, the strength necessary to de-  
21 tached each particles will not be constant and is usually approximated by a log-normal distribution. It is customary  
22 to determine experimentally the adhesion force by calculating the ratio between the number of particles detached by  
23 a certain force and the number of particles initially deposited on the surface. There are many methods for measuring  
24 adhesion strength between particles and surfaces. One common method is centrifugation ([Krupp \[1967\]](#), [Mizes et al.  
25 \[2000\]](#), [Salazar-Banda et al. \[2007\]](#), [Petean and Aguiar \[2015\]](#)), where particles are being detached by centrifugal  
26 forces when the surface on which they are deposited is rotated rapidly. Aerodynamic detachment method ([Matsusaka  
27 and Masuda \[1996\]](#), [Peillon et al. \[2014\]](#), [Brambilla et al. \[2017\]](#)), vibration method ([Ripperger and Hein \[2004\]](#)), or  
28 inertial detachment ([Wanka et al. \[2013\]](#), [Zafar et al. \[2014\]](#)) have also been proposed to measure the adhesion force  
29 distribution of a set of particles deposited on a substrate. Other known methods like electrostatic detachment based  
30 on planar capacitor devices in which particles are exposed to increasing electric fields have been used extensively  
31 ([Cho \[1964\]](#), [Cooper et al. \[1988\]](#), [Takeuchi \[2006\]](#), [Szarek and Dunn \[2007\]](#)). Very recently this method has been  
32 employed specifically for tungsten spherical particles deposited on tungsten substrates with the aim of determining  
33 detachment correlation between particle diameter and electric field detachment threshold ([Riva et al. \[2017\]](#), [Peillon  
34 et al. \[2017\]](#), [Tolias et al. \[2018\]](#)). Such techniques make it possible to obtain the distribution of the adhesion forces  
35 for a large number of particles, thus with a good statistical representation. However, some common drawbacks such  
36 as control of the electric charge on the particles, uniformity of the electric fields, particle shape and spread of particle  
37 size distribution bring certain limitations for quantitative adhesion studies.

38 On the other hand, the colloidal probe technique introduced by [Ducker et al. \[1991\]](#) permits the measurement of the  
39 total adhesion force (or pull-off force) between a single particle and a substrate. Over the years, Atomic Force Mi-  
40 croscopy (AFM) became a reliable method to confront adhesion theoretical models with quantitative measurements  
41 of adhesion forces ([Butt et al. \[2005\]](#), [Leite et al. \[2012\]](#)). Indeed, contact mechanic models such as JKR ([Johnson  
42 et al. \[1971\]](#)), DMT ([Derjaguin et al. \[1975\]](#)) or Maugis - Dugdale (M-D) ([Maugis \[1992\]](#)) as well as van der Waals  
43 based model ([Hamaker \[1937\]](#), [Parsegian \[2005\]](#)) have been consistently tested by means of AFM force spectroscopy

44 technique with common materials such as silica (Olsson et al. [1992], Jones et al. [2002]), alumina (Götzinger and  
45 Peukert [2003]), polystyrene (Gauthier et al. [2013]) copper (Butt et al. [2005]), gold (Heim et al. [2002]) or stainless  
46 steel (Götzinger and Peukert [2004]). Nevertheless, only few work have been initiated to evaluate the adhesion force  
47 with AFM technique between relevant dusts and surfaces one can find in nuclear fusion facilities. To our knowledge,  
48 only few studies (Mokgalapa et al. [2014], Zhang et al. [2015]) between graphene particles with complex geometry  
49 and different types of surfaces found in High Temperature Reactors (HTR) have been performed so far with AFM.  
50 However, in both aforementioned studies, roughness of surfaces and irregularity of particles were not controlled  
51 which makes the comparison with adhesion models difficult. Reduction of adhesion by roughness of surfaces is a  
52 well-documented topic since Fuller and Tabor [1975] conducted systematic studies of roughness effect on the adhe-  
53 sion and suggested taking into account the distribution of heights of substrates in the calculation of adhesive forces.  
54 Further developments based on the Hamaker theory (Hamaker [1937]) were proposed by Rumpf [1990] and later by  
55 Rabinovich et al. [2000b] by considering asperities on the surface as protruding hemispheres or submerged spheres  
56 for the latter. In these van der Waals based theories, surface deformation is not considered contrary to the mechanic  
57 theories of adhesion of JKR/DMT models that take into account the surface of the contact area between the two bodies  
58 under specific external load and the surface energy of adhesion to determine the pull-off force. When applied to rough  
59 surfaces, these smooth-surface models have shown to greatly over-estimate the adhesion force (Götzinger and Peukert  
60 [2003]).

61 In this paper, we focus on direct measurement of adhesion force (or pull-off force) between hard spherical tungsten  
62 particles with sizes in the micrometer range and tungsten surfaces with various roughness using Atomic Force Mi-  
63 croscopy (AFM). The spherical shape of particles is a prerequisite for proper comparison between adhesion force  
64 models and pull-off force experiments. In the first part of this manuscript, van der Waals based theory of adhesion  
65 with the integration of roughness effect will be introduced and domains of applicability of the theory will be dis-  
66 cussed. The second part of the present paper will address the experimental method implemented for the pull-off force  
67 measurements. A special attention has been given to the production of samples with defined shapes and roughness  
68 and the characterization of contacting surfaces during experiments. A wide range of spherical tungsten particles were  
69 produced and studied from 1  $\mu\text{m}$  to 10.5  $\mu\text{m}$  in radius. Likewise, tungsten substrates with three different scales of  
70 roughness were fabricated and analyzed with AFM. In the third part of the paper, results of pull-off force measure-  
71 ments will be presented and a comparison with van der Waals based force models of Rumpf [1990] and Rabinovich  
72 et al. [2000a] is proposed. Estimation of the Hamaker constant for W/W interaction in ambient air is also addressed  
73 in this section.

## 74 1. Theoretical considerations

75 General adhesion of solids is governed by various phenomena such as capillary forces in the presence of water  
76 vapor, electrostatic forces when particles possess electrical charges (friction, radioactivity), hydrogen bonds in case

77 of chemical reactive surfaces and van der Waals forces. In the present study, capillary forces are not discussed and  
 78 are considered as non determinant parameters since measurements were taken at a constant humidity level of 40 %.  
 79 As the study is focused on the adhesion of similar materials (tungsten) and as grafted particles were actually used a  
 80 long time after their fabrication, electrostatic interactions can also be neglected and the following will focus on the  
 81 influence of surface roughness on the adhesion.

### 82 1.1. The Hamaker theory

83 The Hamaker [1937] theory describes interactions between pairs of atoms composing non-deformable macro-  
 84 scopic objects. These atom-atom interactions are additive and ruled by the Hamaker constant and the distance between  
 85 objects. The van der Waals force between a smooth sphere and a smooth planar surface is expressed by the Hamaker  
 86 theory,

$$F_{vdW} = \frac{A \cdot R_p}{6 \cdot z_0^2}, \quad (1)$$

87 with  $A$  the Hamaker constant,  $R_p$  the particle radius and  $z_0$  the distance of closest approach between surfaces. In  
 88 this theory, surfaces in contact are perfectly smooth which leads to consider the closest distance between materials  
 89  $z_0$  as the intermolecular length scale generally around 0.4 nm (Israelachvili [2011]). An early model that integrates  
 90 roughness effect to Hamaker theory by changing the geometry of the problem was introduced by Rumpf [1990].

### 91 1.2. The Rumpf theory

92 The Rumpf model consists of two terms that describe the total van der Waals interaction between a large spherical  
 93 particle and hemispherical asperity protruding a plane surface as depicted in Figure 1. The first term represents direct  
 94 interaction (contact) between the particle and the asperity while the second term stands for “non-contact” interactions  
 95 between the particle and the surface separated by the height of the asperity. The corresponding van der Waals force is  
 96 written as follows:

$$F_{vdW} = \frac{A}{6 \cdot z_0^2} \left[ \frac{r_s \cdot R_p}{r_s + R_p} + \frac{R_p}{(1 + r_s/z_0)^2} \right] \quad (2)$$

97 with  $r_s$  the asperity radius. Rabinovich et al. [2000b] pointed out that with such a geometry, the center of the hemi-  
 98 spherical asperity must be located at the surface which is generally too much simplification for real substrate.

99 In addition, Rabinovich noted that the radius of asperity is difficult to measure while common AFM technique is  
 100 able to measure accurately the height and root-mean-square (*rms*) roughness of surfaces. Hence, Rabinovich *et al.*  
 101 proposed a relationship between the radius of asperity and *rms* roughness defined as follows:

$$r_s = 1.485 \cdot rms. \quad (3)$$

102 Substituting (3) in (2) leads to the following expression:

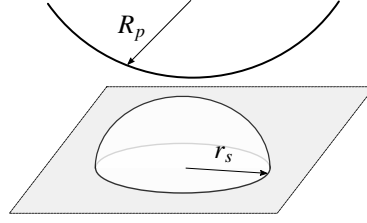


Figure 1: Schematic illustration of the geometry proposed by Rumpf for the interaction of a spherical particle with radius  $R_p$  with an hemispherical asperity of radius  $r_s$ .

$$F_{vdW} = \frac{A \cdot R_p}{6 \cdot z_0^2} \left[ \frac{1}{1 + R_p/(1.485 \cdot rms)} + \frac{1}{(1 + 1.485 \cdot rms/z_0)^2} \right], \quad (4)$$

103 which is referred to by [Rabinovich et al. \[2000b\]](#) as the modified Rumpf's model . When more than one scale  
 104 roughness is considered, the global equivalent roughness of the surface can be calculated as follows:

$$rms = \sqrt{rms_1^2 + rms_2^2}, \quad (5)$$

105 where  $rms_1$  and  $rms_2$  are the average root-mean-square roughnesses of the long and short peak-to-peak distances  
 106 respectively ([Rabinovich et al. \[2000a\]](#)). Figure 2 depicts the evolution of total adhesion forces normalized by the  
 107 radius of the particle using the relation (4) for tungsten particles with radius  $R_p = 2.5 \mu\text{m}$ ,  $5 \mu\text{m}$  and  $10 \mu\text{m}$ , Hamaker  
 108 constant for pure W/W interaction  $A = 49 \cdot 10^{-20} \text{ J}$  given by [Tolias \[2018\]](#) and closest distance approach between  
 109 surfaces  $z_0 = 0.45 \text{ nm}$  ([Israelachvili \[2011\]](#)). Total adhesion force exhibits two distinct regimes depending on the  
 110 surface roughness at the nanoscale. For a  $rms$  roughness above 10 nm, the normalized adhesion is ruled by the  
 111 contact term of the modified Rumpf equation whereas the non-contact interaction between the particle and the surface  
 112 dominates for  $rms$  roughness below 10 nm. As pointed out by [Xie \[1997\]](#), surfaces with such small  $rms$  roughness  
 113 (below 10 nm) will be treated as smooth. As depicted by Figure 2, in the non-contact interaction regime corresponding  
 114 to nanoscale roughness below 10 nm, the normalized adhesion force is independent on the particle radius (second term  
 115 in Eq. 4) and increases when nanoscale roughness decreases. However this observation is not valid for the contact  
 116 adhesion force regime (first term in Eq. 4) where the normalized force decreases as the particle's size increases for a  
 117 given  $rms$  roughness. Indeed, as the particle's radius increases, the minimum normalized adhesion force decreases and  
 118 a shift in the contact component towards higher  $rms$  roughness occurs. This prediction of the modified Rumpf model  
 119 for roughnesses above tens of nanometers has been discussed extensively in the literature ([Göttinger and Peukert](#)  
 120 [\[2003\]](#), [Laitinen et al. \[2013\]](#), [LaMarche et al. \[2017\]](#)) and systematically shows poor agreement with experiment  
 121 underestimating the adhesion force.

### 122 1.3. The Rabinovich model

123 The poor agreement between the Rumpf theory and experiment for large nanoscale roughness has conducted  
 124 [Rabinovich et al. \[2000b\]](#) to further develop the surface geometry by considering that the center of the hemispherical

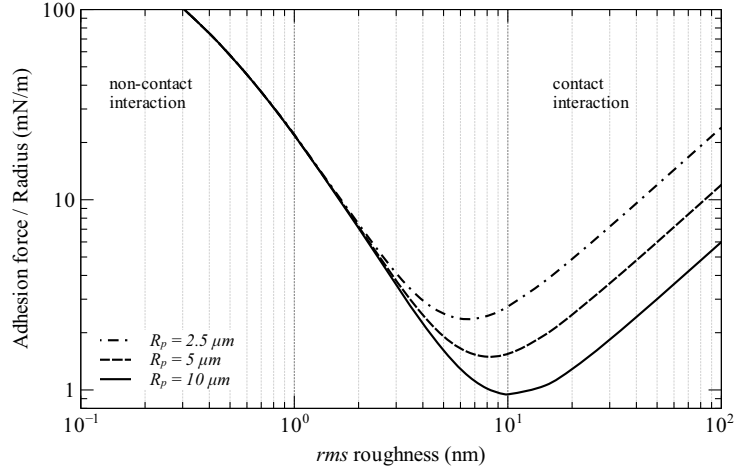


Figure 2: Total adhesion force normalized by the particle radius ( $R_p = 2.5 \mu\text{m}$ ,  $5 \mu\text{m}$  and  $10 \mu\text{m}$ ) using the modified Rumpf model (4) with Hamaker constant of  $49 \cdot 10^{-20} \text{ J}$  (Tolias [2018]) and distance of closest approach  $z_0 = 0.45 \text{ nm}$ .

125 asperity is generally not aligned with the surface but embedded below it. In addition to the height of asperities, a new  
 126 parameter  $\lambda$  referred to as the breadth between asperities has been added to the model.

127 Moreover, authors observed that common surfaces are always composed of a nanoscale roughness superimposed on  
 128 a larger microscale roughness (also referred to as waviness) with much longer peak-to-peak distance. Rabinovich *et al.*  
 129 *et al.* thus incorporated the contribution of two scales of surface roughness, characterized by their root-mean-square  
 130 roughness  $\text{rms}_i$  and peak-to-peak distances  $\lambda_i$ . The total adhesion force is simply the sum of the contribution of the  
 131 adhesion of the particle with the different roughness structures and the underlying plane and is given by Rabinovich  
 132 *et al.* [2000b]:

$$F_a = \frac{A \cdot R_p}{6 \cdot z_0^2} \left[ \frac{1}{1 + 58 \text{rms}_2 R_p / \lambda_2^2} + \frac{1}{(1 + 58 \text{rms}_1 R_p / \lambda_1^2) (1 + 1.82 \text{rms}_2 / z_0)^2} + \frac{z_0^2}{(1 + 1.82 (\text{rms}_1 + \text{rms}_2))^2} \right]. \quad (6)$$

133 Figure 3 depicts such a geometry considering two superimposed roughness as described by Rabinovich. Note that for  
 134 this geometry, the height of the asperity above the average surface plane is not equal to the radius of the asperity and  
 135 its origin is located below the average surface plane.

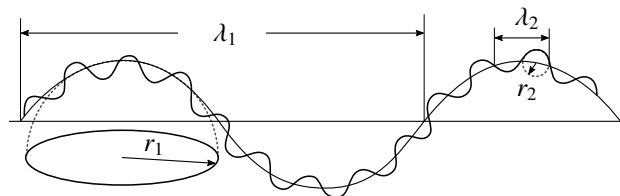


Figure 3: Schematic illustration of the geometry proposed by Rabinovich *et al.* for the interaction of a spherical particle with a surface composed of two scales of roughness.

Eq. (6) is valid as long as the *rms* and wavelength of the two scales roughness remain smaller than the size of the adhering particle. When  $\lambda_1$  becomes comparable to  $R_p$ , the average plane of the surface is incorporated in the large asperities and the third term of eq. (6) can be dropped, yielding:

$$F_a = \frac{A \cdot R_p}{6 \cdot z_0^2} \left[ \frac{1}{1 + 58 \text{rms}_2 R_p / \lambda_2^2} + \frac{1}{(1 + 58 \text{rms}_1 R_p / \lambda_1^2)(1 + 1.82 \text{rms}_2 / z_0)^2} \right]. \quad (7)$$

In such a case ( $\lambda_1 > R_p$ ), the contact term provides the major contribution to the total adhesion force although the non-contact term keeps its influence in the nanoscale roughness regime. This situation is depicted in Figure 4 representing the total adhesion force normalized by the particle radius according to the superimposed roughness (*rms*<sub>2</sub>) while other surface parameters are kept constant. The Hamaker constant and distance of closest approach are identical to the example in Figure 2.

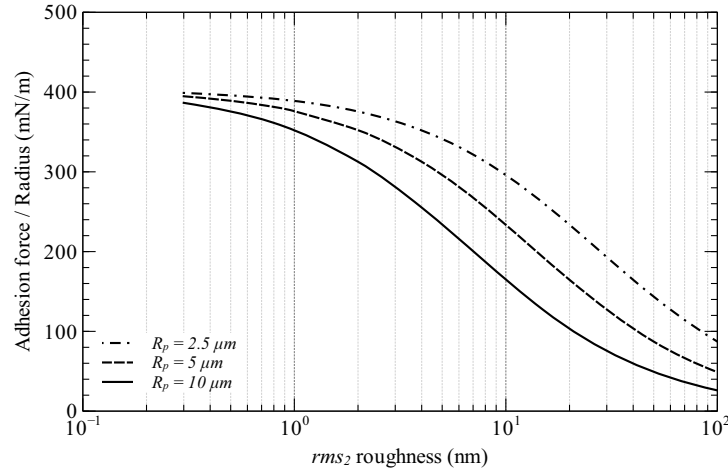


Figure 4: Total adhesion force normalized by the particle radius ( $R_p = 2.5 \mu\text{m}$ ,  $5 \mu\text{m}$  and  $10 \mu\text{m}$ ) using the Rabinovich model with the same parameters of Figure 2 (Hamaker constant of  $49 \cdot 10^{-20}$  J and distance of closest approach  $z_0 = 0.45$  nm).

In contrast with the modified Rumpf model, the Rabinovich model does not predict a minimum value for the total normalized adhesion force but a continuous decrease with the increase of the superimposed roughness of the surface. This eliminates the increase in the normalized adhesion force predicted by the modified Rumpf model for *rms* roughnesses above 10 nm previously described in Figure 2. Moreover, values of normalized adhesion forces appear to be a full order of magnitude greater than calculated with the modified Rumpf model. Although the geometry proposed by Rabinovich shows good results when compared to experiments (Laitinen et al. [2013]), it has some limitations: (i) particles and surfaces that come in contact are regarded as nondeformable under the applied loads. Plastic deformation is thus neglected; (ii) it considers a single point of contact between the particle and the surface which can be different from the equilibrium position. Nevertheless, when using the colloidal AFM technique, particles are fixed under the cantilever and thus not free to move to find more than one contact point. In addition, the use of a hard material such



154 as tungsten (Young's modulus of  $E = 400$  GPa at room temperature) for both the particle and the surface material  
155 reduces to its minimum the plastic deformations that can arise during contact.

## 156 2. Experimental methods

### 157 2.1. Adhesion force measurements

158 Adhesion force measurements have been realized with a Multimode 8 (Bruker™) AFM in PeakForce Quantitative  
159 Nano-Mechanical mode (PF-QNM) in environmental conditions. The measurements were realized between tungsten  
160 spherical particles with different sizes glued onto tip-less CP-FM (Colloidal Probe for Force Modulation) cantilevers  
161 and three different tungsten surfaces with various roughnesses. Samples were cleaned by successive ultrasonic baths  
162 of acetone and ethanol and dried before being mounted in the AFM. For each particle/surface configuration, an AFM  
163 topographic image (see Figure 5-a) with a minimum size of  $10 \times 10 \mu\text{m}^2$  composed of a matrix of  $128 \times 128$  points with  
164 a scanning rate of 0.1 Hz has been realized. A force/distance curve can thus be obtained for each pixel of the adhesion  
165 image. An adhesion force distribution is then extracted from the adhesion image (Figure 5-b) and approximated with  
166 log-normal distribution as shown in Figure 5(c).

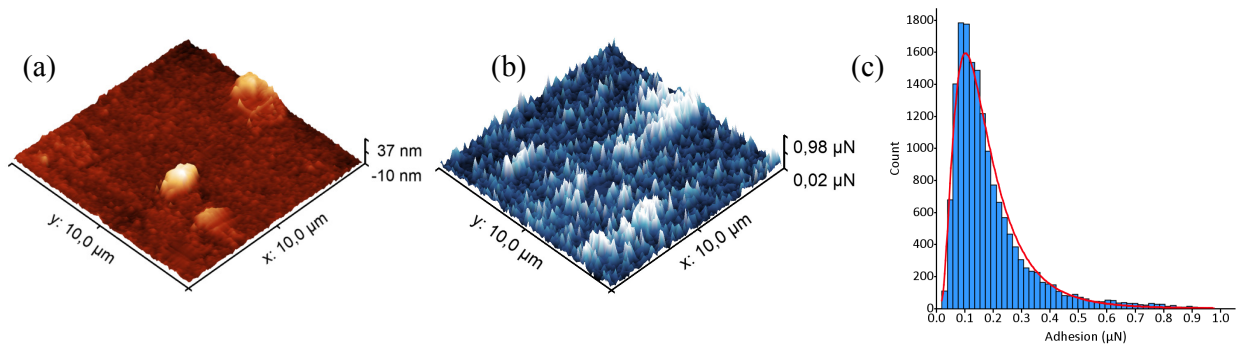


Figure 5: (a) Topographic AFM image ( $10 \times 10 \mu\text{m}^2$ ) obtained in PF-QNM mode with a  $3.9 \mu\text{m}$  tungsten particle. (b) Adhesion image resulting of the PF-QNM scan and (c) adhesion force distribution extracted from the AFM force image with a  $3.9 \mu\text{m}$  radius tungsten particle. The log-normal fit is described by the red continuous line.

167 Repeatability has been tested by measuring twice the adhesion force distribution on the same area ( $10 \times 10 \mu\text{m}^2$ )  
168 on a nanoscale tungsten substrate with the same colloidal probe cantilever and same scanning parameters. Mean  
169 adhesion force of the two measurements is found identical (0.16 % of difference) and the variation (twice the standard  
170 deviation) of each measurement lies around 5 %. For most configurations (particle/substrate), at least three different  
171 regions have been scanned thus giving three log-normal adhesion force distributions. The mean and the spread of  
172 these log-normal adhesion distributions can be then compared with the adhesion force models. It has to be recalled  
173 here that, for each adhesion image, 16384 pull-off force values are obtained giving in a single image a good statistical  
174 representation of the distribution of the adhesion between the particle and a specific substrate.

175 2.2. Materials

176 *Functionalized cantilevers.* Tungsten particles were purchased from Tekna Advanced Materials™ which produces  
177 metallic powders by a RF plasma discharge technique (see Jiang and Boulos [2006]). The Tekna W25 powder comes  
178 with a broad size distribution with spherical particles with radius between 4  $\mu\text{m}$  and 15  $\mu\text{m}$ . In order to perform the  
179 grafting of spherical particles with best control, a wet sieving method has been used in order to reduce the broadness  
180 of the mean particle size. After this step, batches of powders with narrower particle size distributions were used  
181 for functionalization of the cantilevers. For smaller particle radii, i.e. between 1  $\mu\text{m}$  and 4  $\mu\text{m}$ , a specific tungsten  
182 powder from Alfa Aesar® with a median radius of 2.2  $\mu\text{m}$  and a geometric standard deviation of 1.6 has been sent to  
183 Tekna Advanced Materials™ to undergo the same spheroidization procedure. Tungsten spherical particles of desire  
184 sizes were then grafted on AFM tip-less cantilevers using optical microscope, micromanipulator and epoxy following  
185 method introduced by Ducker et al. [1991] and well detailed by Gan [2007]. Grafted cantilevers were verified by SEM  
186 analysis before and after pull-off force experiments in order to estimate their radii and check that no contamination  
187 was present on the particles. Figure 6 shows SEM micrographs of these particles once attached onto AFM cantilevers.  
188 Seven particle radii have been investigated in this study: 1  $\mu\text{m}$ , 1.8  $\mu\text{m}$ , 3  $\mu\text{m}$ , 3.9  $\mu\text{m}$ , 5.5  $\mu\text{m}$ , 7.5  $\mu\text{m}$  and 10.5  $\mu\text{m}$ .  
189 SEM analysis also emphasized that no plastic deformations were visible after pull-off force experiments. The spring  
190 constant of the functionalized cantilevers was measured using the Thermal Tune method provided by the Bruker AFM  
191 software. The thermal method calibrates the spring constant of a cantilever by fitting the power spectral density of the  
192 cantilever fluctuations with a known Lorentzian curve. The calibration procedure has been repeated three times for  
193 each cantilever in order to have the variation of the spring constant. Note that tungsten spherical particles were added  
194 to the cantilevers before spring constants were determined. The radii of the tungsten spheres and the corresponding  
195 spring constants of the cantilevers are provided in Table 1.

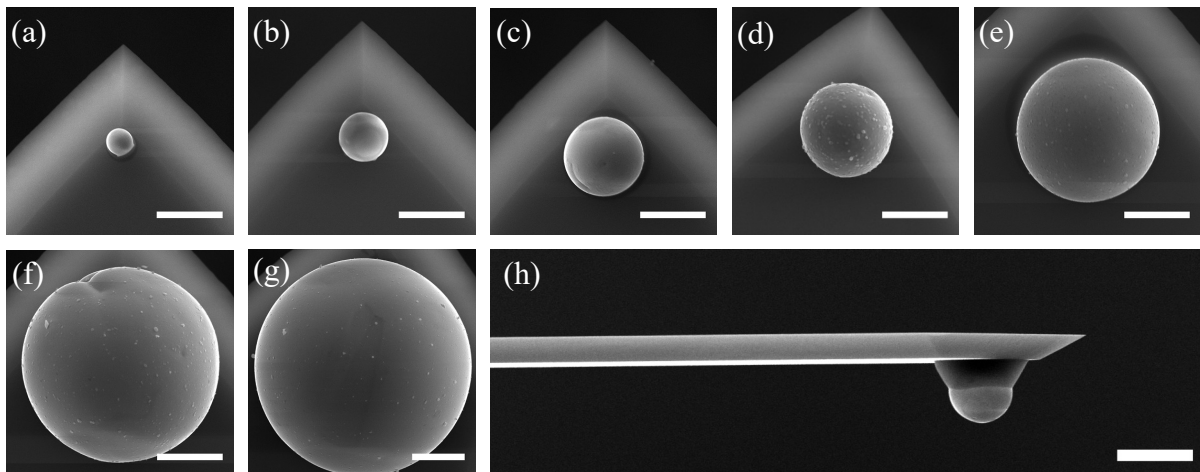


Figure 6: SEM micrographs of tungsten spherical particles grafted onto tip-less cantilevers. Sphere radii are (a) 1  $\mu\text{m}$ , (b) 1.8  $\mu\text{m}$ , (c) 3  $\mu\text{m}$ , (d) 3.9  $\mu\text{m}$ , (e) 5.5  $\mu\text{m}$ , (f) 7.5  $\mu\text{m}$  and (g) 10.5  $\mu\text{m}$ . Side view of the 3.9  $\mu\text{m}$  sphere (h) is also presented. Scale bars are 10  $\mu\text{m}$  in length.

Table 1: Radii of tungsten spheres attached to the cantilevers measured by SEM and spring constants of the cantilevers with particles attached.

réf. Figure 6	(a)	(b)	(c)	(d)	(e)	(f)	(g)
Particle radius ( $\mu\text{m}$ )	$1 \pm 0.05$	$1.8 \pm 0.05$	$3 \pm 0.05$	$3.9 \pm 0.1$	$5.5 \pm 0.1$	$7.5 \pm 0.1$	$10.5 \pm 0.1$
Spring constant (N/m)	$2.53 \pm 0.04$	$2.69 \pm 0.03$	$2.22 \pm 0.12$	$1.92 \pm 0.06$	$1.89 \pm 0.11$	$2.29 \pm 0.16$	$3.03 \pm 0.18$

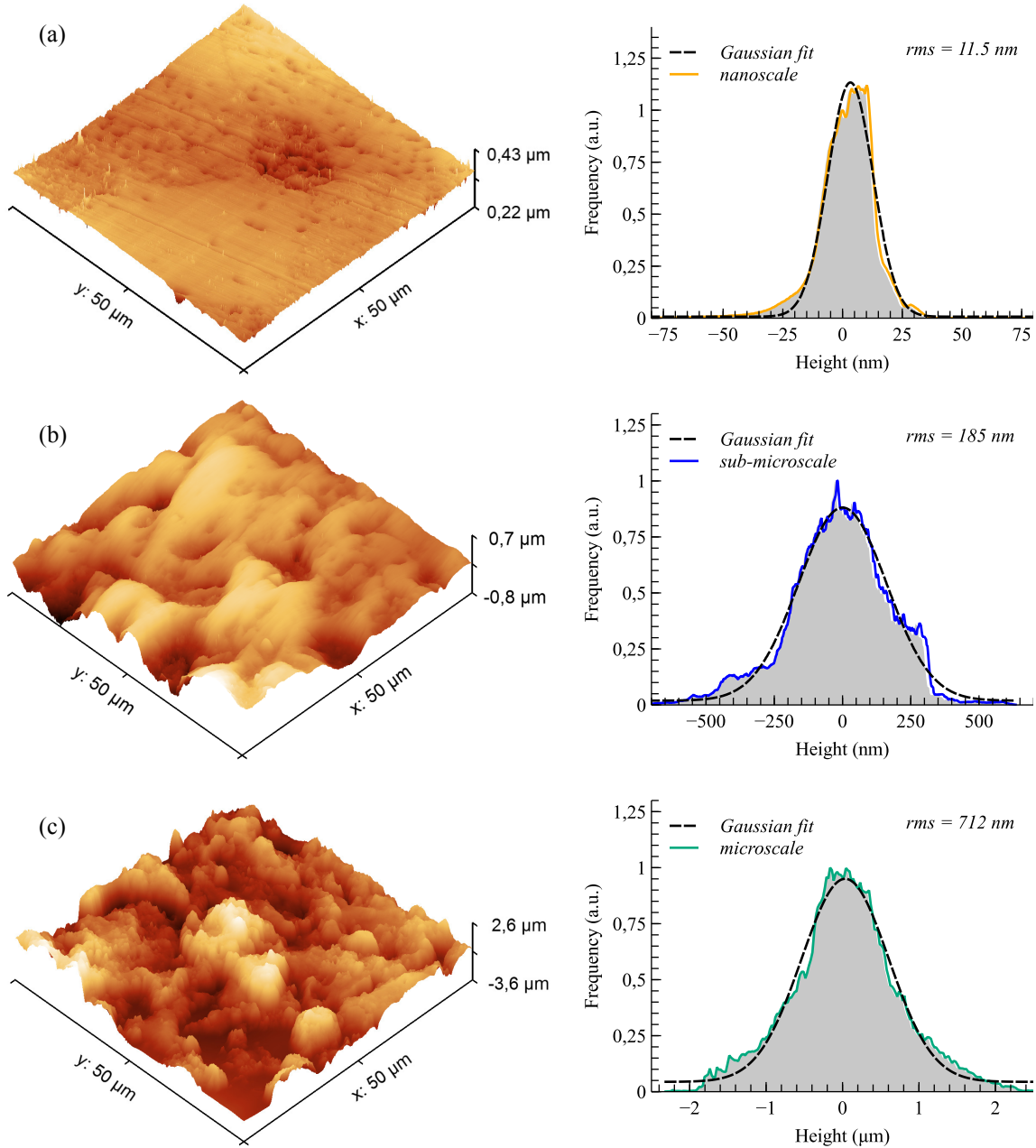


Figure 7: AFM three-dimensional images ( $50 \times 50 \mu\text{m}^2$ ) of (a) the nanoscale tungsten surface, (b) the sub-microscale tungsten surface and (c) the microscale tungsten surface used in the pull-off force measurements. Height histograms of the three substrates are represented together with Gaussian fits (discontinuous black lines).

196 *Surface characterization.* Three tungsten surfaces with different roughnesses and textures have been used in this  
 197 study. Two bulk tungsten substrates were polished in order to reach specific roughness. The first one has been  
 198 mirror polished using different grades of SiC papers and diamond paste to reach a *rms* surface roughness of the  
 199 order 10 nm. It will be referred as nanoscale tungsten substrate in the following. The second one has been hand-  
 200 polished and exhibits a *rms* surface roughness in the range 100 – 200 nm (referred as sub-microscale surface in the  
 201 following). The third tungsten substrate has been exposed to high temperatures (above 1000 °C) by He plasma using  
 202 radiofrequency (RF) hollow cathode discharge technique described by [Stancu et al. \[2017\]](#) (referred as microscale  
 203 surface in the following). The dimensions of the tungsten substrates are approximately  $5 \times 5 \text{ mm}^2$ . AFM topographic  
 204 measurements in ScanAsyst mode (Bruker) with standard Scanasyst probes have been performed on the three surfaces  
 205 and are depicted in Figure 7. The scans are  $50 \times 50 \mu\text{m}$  in size with a resolution of  $2048 \times 2048$  data points. Height  
 206 histograms of the three substrates are represented in Figure 7 together with Gaussian fits that permits to calculate the  
 207 *rms* roughnesses (standard deviation of the height distributions) of each substrate. The root-mean-square roughness  
 208 (also referred as  $R_q$ ) is defined by:

$$R_q = \sqrt{\frac{1}{MN} \sum_{i=1}^M \sum_{j=1}^N (z(i, j))^2}, \quad (8)$$

209 with  $M \times N$  a matrix containing the height data  $z(i, j)$ . The calculated roughnesses ( $R_q$ ) are 11.5 nm, 185 nm and 712  
 210 nm for the nanoscale surface, the sub-microscale surface and the microscale surface respectively.

### 211 3. Results and Discussion

#### 212 3.1. Estimation of the Hamaker constant

213 In this section we present the method we used to measure the Hamaker constant for W/W interaction in ambient  
 214 air. The cantilever with the grafted  $10.5 \mu\text{m}$  radius particle has been used to performed pull-off measurements in 20  
 215 different locations on the nanoscale W substrate. For this particular measurement, simple force-distance curves were  
 216 obtained and analyzed in each location. Using the classical expression of van der Waals forces given by Eq. (1)  
 217 and taking the closest distance  $z_0 = 0.45 \text{ nm}$ , we found an average Hamaker constant of  $19.9 \pm 2 \times 10^{-20} \text{ J}$  which is  
 218 two times below the theoretical values of  $A_H$  calculated using Lifshitz theory, i.e.  $40 - 50 \times 10^{-20} \text{ J}$  ([Tolias \[2018\]](#)).  
 219 The low values obtained experimentally can be explained by the influence of roughness of both contacting surfaces.  
 220 Indeed, the nanoscale tungsten substrate exhibits a nanoscale roughness of 11.5 nm. Identically, the tungsten particle  
 221 possesses its own surface roughness that we have calculated after mapping the top of the particle with AFM tapping  
 222 mode (image dimension of  $2 \times 2 \mu\text{m}^2$ ). Figure 8 depicts a  $2 \mu\text{m}$  wide line profile extracted from the AFM topography  
 223 image taken at the top of the  $10.5 \mu\text{m}$  particle. By substituting the fit parabola (red line in Figure 8) to the measured  
 224 profile (blue line), we are able to plot the equivalent roughness that would be measured on a flat surface. In this case,  
 225 the W particle shows a sub-nanoscale structured surface with a *rms* roughness of 0.29 nm.

226 Although such atomic-scale roughness has proved to reduce adhesion by nearly an order of magnitude compared  
 227 to atomically flat surface ([Jacobs et al. \[2013\]](#)), in the present interaction the separation distance between the colloidal

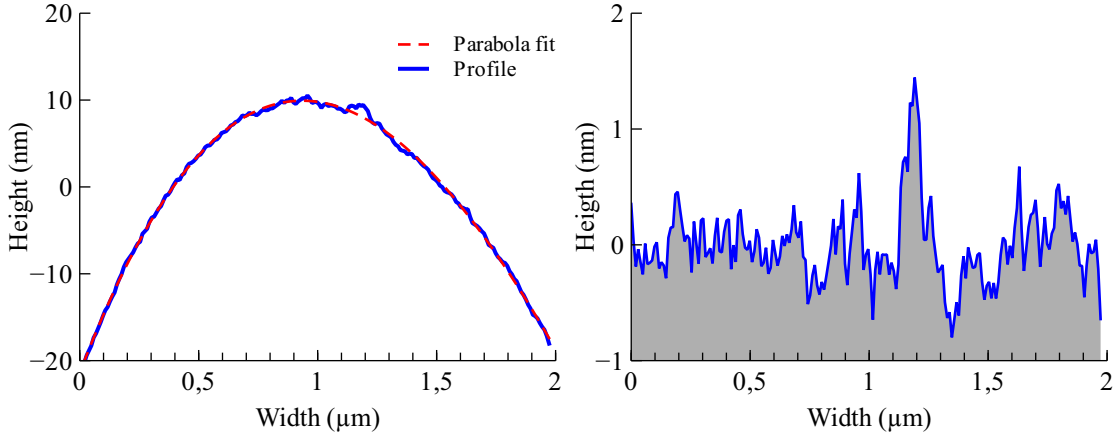


Figure 8: (top) Line profile at the top of the 10.5  $\mu\text{m}$  particle (blue line) and parabola fit (red line). (bottom) Roughness profile of the top of the particle after removal of the parabolic fit.

228 probe and the substrate is governed by the nanoscale roughness of the latter. In order to account for the roughness  
 229 effect in the calculation of the Hamaker constant, we use the classical formula of the Rabinovich model presented in  
 230 section I of this paper:

$$A_{exp} = \frac{6 \cdot F_{exp} \cdot z_0^2}{R_p} \left[ \frac{1}{1 + 58\text{rms}_2 R_p / \lambda_2^2} + \frac{1}{(1 + 58\text{rms}_1 R_p / \lambda_1^2)(1 + 1.82\text{rms}_2 / z_0)^2} \right]^{-1}. \quad (9)$$

231 The experimental Hamaker constants obtained with the classical formula of Hamaker and the Rabinovich model  
 232 taking into account nanoscale roughness are plotted in Figure 9. The average experimental Hamaker constant obtained  
 233 when taking into account the nanoscale roughness of the substrate is  $37 \pm 3.5 \times 10^{-20}$  J. As can be seen from Figure  
 234 9, the adhesion measurements are consistent and repeatable with a fluctuation of 10 % over all the measured data.

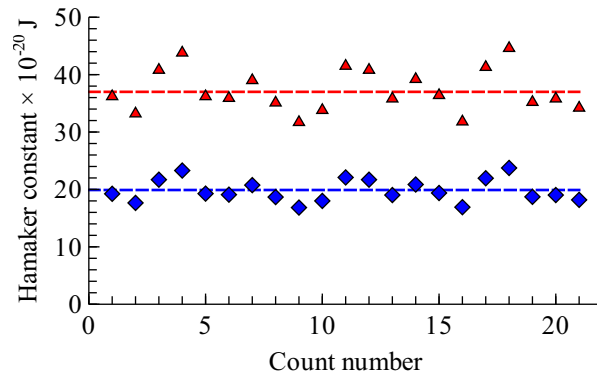


Figure 9: Measured Hamaker constant using a tungsten spherical particle of 10.5  $\mu\text{m}$  radius and nanoscale tungsten surface with the classical formula of Hamaker (blue diamonds) and the model of Rabinovich with roughness correction (red triangles).

235 The experimental values of Hamaker constant obtained with pull-off force data and adjusted with the Rabinovich

236 model are in good agreement with the theoretical value of Hamaker constant for W/W interaction considering the  
 237 experimental conditions (measurements were performed in ambient air) and the repeatability of the technique. More-  
 238 over, it is worth mentioning that pure tungsten is not chemically stable in ambient conditions and it is well known that  
 239 a thin  $\text{WO}_3$  oxide layer ( $\approx 3-6$  nm) forms at the surface of tungsten material (see Peillon et al. [2017]). Such an oxide  
 240 layer adds to the complexity of the measurement for a pure W/W adhesion study and the determination of van der  
 241 Waals interaction by modifying the Hamaker constant of the material. Nevertheless, since all the force measurements  
 242 presented in this paper were realized in ambient air, we will consider an Hamaker constant of  $A_{exp} = 37 \pm 3.5 \times 10^{-20}$   
 243 J in the following.

### 244 3.2. Comparison with the Rabinovich model

245 We present in this section the mean and standard deviation parameters of the adhesion force distributions obtained  
 246 for each particle size and the three different tungsten substrates. Measurements and the outcome of the Rabinovich  
 247 model are plotted in Figures 10, 11 and 12 using the surface parameters given in table 2. These parameters were  
 248 extracted from AFM topography measurements presented in Figure 7.

Table 2: Surface parameters (in nm) used with the Rabinovich model

Samples	$\lambda_1$	$rms_1$	$\lambda_2$	$rms_2$
nanoscale	2780	9.6	1500	3.2
sub-microscale	12800	130	650	21
microscale	2130	717	300	27

249 Derivations of adhesion forces with the Rabinovich model were performed with a minimal separation distance  
 250  $z_0 = 0.45$  nm and the experimental Hamaker constant estimated previously  $A_{exp} = 37 \times 10^{-20}$  J and are represented by  
 251 the continuous lines in Figures 10, 11 and 12. We also performed the calculations of adhesion forces with the minimum  
 252 ( $A_{min} = 33.5 \times 10^{-20}$  J) and maximum ( $A_{max} = 40.5 \times 10^{-20}$  J) Hamaker constants deduced from the measurement in  
 253 Section 3.1. These limit values are denoted  $A_{\pm 10\%}$  and are depicted by the dashed lines in Figures 10, 11 and 12.

254 *Tungsten surface with nanoscale roughness.* Adhesion measurements obtained with the nanoscale tungsten surface  
 255 are presented in Figure 10 together with the Rabinovich model derivations.

256 Experimental adhesion measurements on the nanoscale roughness tungsten surface with tungsten particles from 1  
 257  $\mu\text{m}$  to 10.5  $\mu\text{m}$  radius exhibit mean adhesion forces between 300 nN and 1700 nN. Standard deviations of the mean  
 258 adhesion forces are below 5 % except for the 3.9  $\mu\text{m}$  radius particle and the larger 10.5  $\mu\text{m}$  radius particle where the  
 259 standard deviations are 22 % and 10 % respectively. In comparison, the classical Hamaker formula for the derivation  
 260 of the van der Waals force (eq. 1) between a sphere and a plane gives 3 350 nN for the 10.5  $\mu\text{m}$  radius particle  
 261 which is two times the experimental value. This two times overestimate by the model is clearly related to the surface  
 262 roughness. This is confirmed by Figure 10 where the Rabinovich model is consistent with data for all particle sizes  
 263 tested except for the 3.9  $\mu\text{m}$  particle radius.

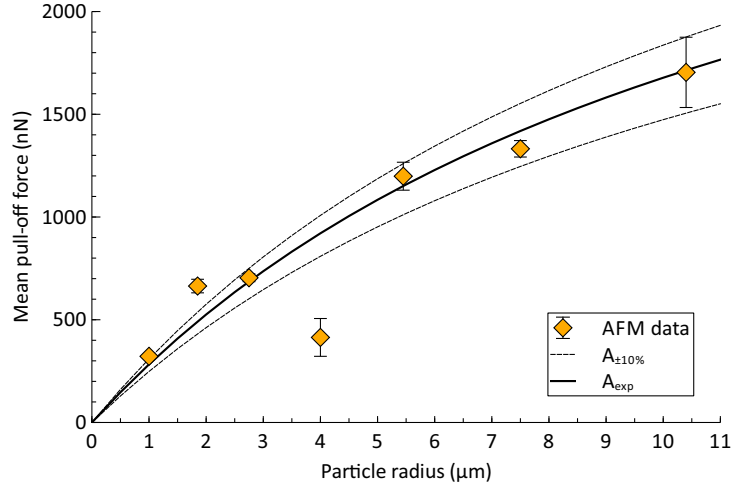


Figure 10: Mean adhesion forces versus particle radius with the nanoscale tungsten surface. Continuous and dashed lines represent the Rabinovich model derivations with the experimental Hamaker constant  $A_{exp}$  and its 10% variation.

264 *Effect of particle roughness.* Indeed, the experimental mean adhesion force with the 3.9  $\mu\text{m}$  particle radius is 414 nN  
 265 which is two times lower than the predicted adhesion by the Rabinovich model. Such a drop in the adhesion can again  
 266 be explained by the surface roughness of the particle itself. To confirm this hypothesis, we measured the topography  
 267 of the summit of this particle with the AFM. A nanostructured surface was found with a  $rms$  of 12.6 nm. Such  
 268 an important roughness cannot be ignored and have to be incorporated in the Rabinovich derivation. To do so, we  
 269 simplified the problem by considering that the roughness of the particle  $rms_p$  adds-up to the superimposed nanoscale  
 270 roughness  $rms_2$  of the substrate. We can thus rewrite the superimposed roughness used by the Rabinovich model as  
 271 follows:  $rms_3 = \sqrt{rms_p^2 + rms_2^2}$  which gives 13 nm. With this new roughness value, the derivation of the adhesion  
 272 force for the 3.9  $\mu\text{m}$  particle radius gives 440 nN which is much closer to the observed experimental value considering  
 273 the variations observed ( $\approx 10\%$ ). On the other hand, derivations using the modified Rumpf model (eq. 2) and the  
 274 same parameters (i.e. closest distance between surfaces  $z_0$  and Hamaker constant  $A_{exp}$ ) were carried out with the  
 275  $rms$  roughness of 11.5 nm and returned adhesion values between 10 nN and 30 nN which are far from experimental  
 276 data. As discussed previously in Figure 2, the minimal value of normalized adhesion forces for micron-sized particles  
 277 predicted by the modified Rumpf model occurs precisely for  $rms$  roughness close to 10 nm. For such a range of  
 278 roughness, we show that the modified Rumpf model greatly underestimate adhesion forces and should not be used in  
 279 that case.

280 *Tungsten surface with sub-microscale roughness.* Adhesion measurements obtained with the sub-microscale tungsten  
 281 surface are presented in Figure 11 together with the Rabinovich and Rumpf model calculations.

282 Experimental adhesion measurements on the tungsten sub-microscale roughness surface with tungsten particles from  
 283 1  $\mu\text{m}$  to 10.5  $\mu\text{m}$  radius exhibit mean adhesion forces between 10 nN and 115 nN which is one order of magnitude  
 284 below data obtained with the tungsten nanoscale surface. On the other hand, the standard deviations of the mean

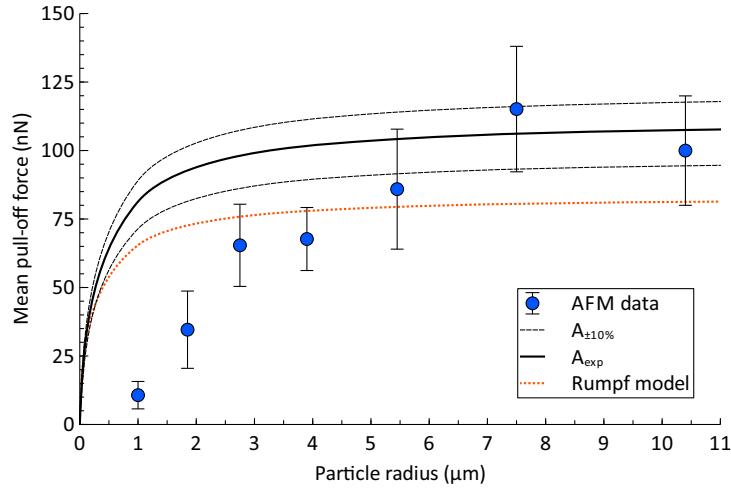


Figure 11: Mean adhesion forces versus particle radius with the sub-microscale tungsten surface. Continuous and dashed lines represent the Rabinovich model derivations with the experimental Hamaker constant  $A_{exp}$  and its 10% variation.

285 adhesion forces are much larger with values between 19 % and 46 %. Rabinovich model is consistent with data for  
 286 particle above  $5.5 \mu\text{m}$  in radius but fails to describe the adhesion reduction observed when the particle radius is below  
 287  $5 \mu\text{m}$ . This specific feature remains unexplained. Using the same parameters and the *rms* roughness of 185 nm for the  
 288 sub-microscale tungsten surface, we plotted the modified Rumpf model calculations in Figure 11. In this case, results  
 289 are of same order of magnitude with experimental data. However, the Rumpf model still underestimate by 25 % the  
 290 adhesion forces compared to Rabinovich derivations.

291 *Tungsten surface with microscale roughness.* Adhesion measurements obtained with the microscale tungsten surface  
 292 are presented in Figure 12 together with the Rabinovich model calculations.

293 Experimental adhesion measurements on the microscale roughness tungsten surface with tungsten particles from  $1 \mu\text{m}$   
 294 to  $10.5 \mu\text{m}$  radius exhibit mean adhesion forces between 10 nN and 30 nN. Standard deviations of the mean adhesion  
 295 forces are consequent and above 80 % for all the mean adhesion forces. In such a case with a very textured substrate  
 296 composed of a microscale roughness, adhesion of micrometer particles becomes independent with the particle size as  
 297 previously noticed by Laitinen et al. [2013]. In this case, surface roughness appears to play the dominant role whereas  
 298 particle size has a secondary influence on adhesion force. This behavior is well described by the Rabinovich model  
 299 which returns values that are the same order of magnitude than experimental data. In contrast, derivations using the  
 300 modified Rumpf model with the *rms* roughness of 712 nm returned adhesion values between 103 nN and 293 nN  
 301 which are one order of magnitude higher than experimental data.



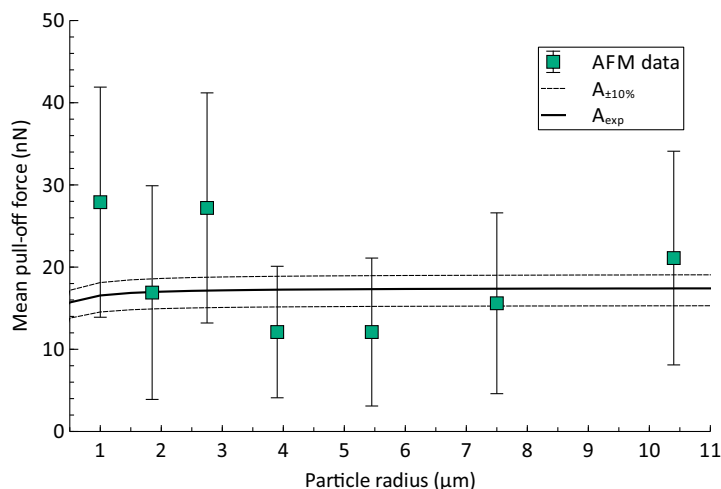


Figure 12: Mean adhesion forces versus particle radius with the microscale tungsten surface. Continuous and dashed lines represent the Rabinovich model derivations with the experimental Hamaker constant  $A_{exp}$  and its 10% variation.

#### 4. Conclusion

Adhesion forces between tungsten spherical microparticles with radii from  $1 \mu\text{m}$  to  $10.5 \mu\text{m}$  and tungsten substrates with different roughnesses have been measured in ambient air using the Atomic Force Microscopy (AFM) colloidal probe technique. Mean roughnesses of the tungsten substrates were measured by AFM and were ranked in three categories i.e. nanoscale, sub-microscale and microscale roughnesses. Experimental Hamaker constant of  $37 \pm 3.5 \times 10^{-20} \text{ J}$  has been obtained using a spherical tungsten particle of  $10.5 \mu\text{m}$  in radius and a tungsten substrate with nanoscale root-mean-square roughness of  $rms = 11.5 \text{ nm}$ . Pull-off force measurements with a nanoscale tungsten substrate (nanoscale  $rms$ ) and microparticles with radii from  $1 \mu\text{m}$  to  $10.5 \mu\text{m}$  gave adhesion forces in the range  $300 \text{ nN}$  to  $1700 \text{ nN}$ . On the other hand, it was shown that larger roughness in the micrometer range induces a two orders of magnitude decrease on the adhesion of the tungsten microparticles compared to the tungsten surface with nanoscale roughness. Sub-micrometer surface roughness ( $rms = 185 \text{ nm}$ ) exhibited adhesion forces in the range  $10 \text{ nN}$  to  $115 \text{ nN}$  in accordance with both the Rabinovich and the Rumpf models. Moreover, we have also shown that:

- Comparison with the van der Waals-based adhesion force model of Rabinovich showed quantitative agreement with experimental pull-off forces for particles with radii between  $1 \mu\text{m}$  and  $10.5 \mu\text{m}$  for smooth surfaces ( $rms \approx 10 \text{ nm}$ ) but also for very rough substrates with a  $rms$  roughness close to the micrometer range.
- For all the configurations tested, we demonstrated the predictive accuracy of the Rabinovich model when definition of the surface roughness is carried out with care.
- For microscale roughness, measurements have shown that dependency of adhesion force with particle size (in the micrometer range) has a secondary influence compared to the roughness of surfaces.

321 The good predictions of the Rabinovich model throughout the range of micron-sized particles and *rms* roughnesses  
322 studied makes it a good substitute to classical empirical correlations (for example the correlation of [Biasi \[2001\]](#))  
323 used in common resuspension models like the Rock'n roll model of [Reeks and Hall \[2001\]](#) by placing the roughness  
324 of the substrate on which particles are deposited as a key parameter for removal predictions as recently stated by  
325 [Henry and Minier \[2018\]](#). When available, experimental adhesion force distributions obtained by AFM can replace  
326 mathematical description of adhesion forces used in numerical codes for resuspension predictions like in [Guingo  
327 and Minier \[2008\]](#), [Benito et al. \[2015\]](#). Such combination between adhesion force distribution measured by AFM  
328 colloidal probe technique and a resuspension model is intended to be tested by the authors in a future work.

### 329 **Acknowledgments**

330 This work has been carried out within the framework of the EUROfusion Consortium and has received funding  
331 under grant number AWP17-ENR-MFE-CEA-10. The views and opinions expressed herein do not necessarily reflect  
332 those of the European Commission. The authors thank L.O Heim from SQUBE Company (Germany) for the grafting  
333 of particles onto cantilevers.

- 334 Benito, J., Aracena, K., Uñac, R., Vidales, A., and Ippolito, I. (2015). Monte Carlo modelling of particle resuspension on a flat surface. *Journal of  
335 Aerosol Science*, 79:126–139.
- 336 Biasi, L. (2001). Use of a simple model for the interpretation of experimental data on particle resuspension in turbulent flows. *Aerosol Science*,  
337 page 26.
- 338 Brambilla, S., Speckart, S., and Brown, M. J. (2017). Adhesion and aerodynamic forces for the resuspension of non-spherical particles in outdoor  
339 environments. *Journal of Aerosol Science*, 112:52–67.
- 340 Butt, H.-J., Cappella, B., and Kappl, M. (2005). Force measurements with the atomic force microscope: Technique, interpretation and applications.  
341 *Surface Science Reports*, 59(1-6):1–152.
- 342 Cho, A. Y. H. (1964). Contact Charging of Micron-Sized Particles in Intense Electric Fields. *Journal of Applied Physics*, 35(9):2561–2564.
- 343 Cooper, D. W., Wolfe, H. L., and Miller, R. J. (1988). Electrostatic Removal of particles from surfaces. In *Particles on Surfaces 1*, Plenum Press,  
344 page 11. K. L. Mittal (éd.), New York.
- 345 Derjaguin, B., Muller, V., and Toporov, Y. (1975). Effect of contact deformations on the adhesion of particles. *Journal of Colloid and Interface  
346 Science*, 53(2):13.
- 347 Ducker, W. A., Senden, T. J., and Pashley, R. M. (1991). Direct measurement of colloidal forces using an atomic force microscope. *Nature*,  
348 353:239–241.
- 349 Fuller, K. N. G. and Tabor, D. (1975). The Effect of Surface Roughness on the Adhesion of Elastic Solids. *Proceedings of the Royal Society A:  
350 Mathematical, Physical and Engineering Sciences*, 345(1642):327–342.
- 351 Gan, Y. (2007). Invited Review Article: A review of techniques for attaching micro- and nanoparticles to a probe's tip for surface force and  
352 near-field optical measurements. *Review of Scientific Instruments*, 78(8):081101.
- 353 Gauthier, e., Alvo, e., Dejeu, o., Tamadate, B., Rougeot, P., and Regnier (2013). Analysis and Specificities of Adhesive Forces Between Microscale  
354 and Nanoscale. *IEEE Transactions on Automation Science and Engineering*, 10(3):562–570.
- 355 Guingo, M. and Minier, J.-P. (2008). A new model for the simulation of particle resuspension by turbulent flows based on a stochastic description  
356 of wall roughness and adhesion forces. *Journal of Aerosol Science*, 39(11):957–973.
- 357 Götzinger, M. and Peukert, W. (2003). Dispersive forces of particle–surface interactions: direct AFM measurements and modelling. *Powder  
358 Technology*, 130(1-3):102–109.

359 Götzing, M. and Peukert, W. (2004). Particle Adhesion Force Distributions on Rough Surfaces. *Langmuir*, 20(13):5298–5303.

360 Hamaker, H. (1937). The London—van der Waals attraction between spherical particles. *Physica*, 4(10):1058–1072.

361 Heim, L. O., Ecke, S., Preuss, M., and Butt, H.-J. (2002). Adhesion forces between individual gold and polystyrene particles. *Journal of Adhesion*  
362 *Science and Technology*, 16(7):829–843.

363 Henry, C. and Minier, J.-P. (2018). Colloidal particle resuspension: On the need for refined characterisation of surface roughness. *Journal of*  
364 *Aerosol Science*, 118:1–13.

365 Israelachvili, J. N. (2011). *Intermolecular and Surface Forces*. Academic Press.

366 Jacobs, T. D. B., Ryan, K. E., Keating, P. L., Grierson, D. S., Lefever, J. A., Turner, K. T., Harrison, J. A., and Carpick, R. W. (2013). The Effect of  
367 Atomic-Scale Roughness on the Adhesion of Nanoscale Asperities: A Combined Simulation and Experimental Investigation. *Tribology Letters*,  
368 50(1):81–93.

369 Jiang, X.-L. and Boulos, M. (2006). Induction plasma spheroidization of tungsten and molybdenum powders. *Transactions of Nonferrous Metals*  
370 *Society of China*, 16(1):13–17.

371 Johnson, K. L., Kendall, K., and Roberts, A. D. (1971). Surface energy and the contact of elastic solids. *Proceedings of the Royal Society A:*  
372 *Mathematical, Physical and Engineering Sciences*, 324:301–313.

373 Jones, R., Pollock, H. M., Cleaver, J. A. S., and Hodges, C. S. (2002). Adhesion Forces between Glass and Silicon Surfaces in Air Studied by  
374 AFM: Effects of Relative Humidity, Particle Size, Roughness, and Surface Treatment. *Langmuir*, 18(21):8045–8055.

375 Krasheninnikov, S. I., Smirnov, R. D., and Rudakov, D. L. (2011). Dust in magnetic fusion devices. *Plasma Physics and Controlled Fusion*,  
376 53(8):083001.

377 Krupp, H. (1967). Particle adhesion: theory and experiment. *Adv. Colloid Interface Sci.*, 1:111-239.

378 Laitinen, O., Bauer, K., Niinimäki, J., and Peuker, U. (2013). Validity of the Rumpf and the Rabinovich adhesion force models for alumina  
379 substrates with nanoscale roughness. *Powder Technology*, 246:545–552.

380 LaMarche, C. Q., Leadley, S., Liu, P., Kellogg, K. M., and Hrenya, C. M. (2017). Method of quantifying surface roughness for accurate adhesive  
381 force predictions. *Chemical Engineering Science*, 158:140–153.

382 Leite, F. L., Bueno, C. C., Da Róz, A. L., Ziemath, E. C., and Oliveira, O. N. (2012). Theoretical Models for Surface Forces and Adhesion and  
383 Their Measurement Using Atomic Force Microscopy. *International Journal of Molecular Sciences*, 13(12):12773–12856.

384 Matsusaka, S. and Masuda, H. (1996). Particle Reentrainment from a Fine Powder Layer in a Turbulent Air Flow. *Aerosol Science and Technology*,  
385 24(2):69–84.

386 Maugis, D. (1992). Adhesion of spheres: The JKR-DMT transition using a dugdale model. *Journal of Colloid and Interface Science*, 150(1):243–  
387 269.

388 Mizes, H., Ott, M., Eklund, E., and Hays, D. (2000). Small particle adhesion: measurement and control. *Colloids and Surfaces A: Physicochemical*  
389 *and Engineering Aspects*, 165(1-3):11–23.

390 Mokgalapa, N. M., Ghosh, T. K., and Loyalka, S. K. (2014). Graphite Particle Adhesion to Hastelloy X: Measurements of the Adhesive Force with  
391 an Atomic Force Microscope. *Nuclear Technology*, 186(1):45–59.

392 Olsson, L., Tengvall, P., Wigren, R., and Erlandsson, R. (1992). Interaction forces between a tungsten tip and methylated SiO<sub>2</sub> surfaces studied  
393 with scanning force microscopy. *Ultramicroscopy*, 42-44:73–79.

394 Parsegian, V. A. (2005). *Van der Waals Forces: A Handbook for Biologists, Chemists, Engineers, and Physicists*. Cambridge University Press,  
395 Cambridge.

396 Peillon, S., Roynette, A., Grisolia, C., and Gensdarmes, F. (2014). Resuspension of carbon dust collected in Tore Supra and exposed to turbulent  
397 airflow: Controlled experiments and comparison with model. *Fusion Engineering and Design*, 89(11):2789–2796.

398 Peillon, S., Sow, M., Grisolia, C., Miserque, F., and Gensdarmes, F. (2017). Mobilization of tungsten dust by electric forces and its bearing on  
399 tritiated particles in the ITER tokamak. *Journal of Electrostatics*, 88:111–115.

400 Petean, P. and Aguiar, M. (2015). Determining the adhesion force between particles and rough surfaces. *Powder Technology*, 274:67–76.

401 Rabinovich, Y. I., Adler, J. J., Ata, A., Singh, R. K., and Moudgil, B. M. (2000a). Adhesion between Nanoscale Rough Surfaces : measurements

402 and comparison with theory. *Journal of Colloid and Interface Science*, 232(1):17–24.

403 Rabinovich, Y. I., Adler, J. J., Ata, A., Singh, R. K., and Moudgil, B. M. (2000b). Adhesion between Nanoscale Rough Surfaces : Role of asperity  
404 geometry. *Journal of Colloid and Interface Science*, 232(1):10–16.

405 Reeks, M. W. and Hall, D. (2001). Kinetic models for particle resuspension in turbulent flows: theory and measurement. *Aerosol Science*, page 31.

406 Ripperger, S. and Hein, K. (2004). Measurement of Adhesion Forces between Particles and Rough Substrates in Air with the Vibration Method.  
407 *KONA Powder and Particle Journal*, 22(0):121–133.

408 Riva, G., Tolia, P., Ratynskaia, S., Daminelli, G., Donde, R., De Angeli, M., Vassallo, E., and Pedroni, M. (2017). Adhesion measurements for  
409 tungsten dust deposited on tungsten surfaces. *Nuclear Materials and Energy*, 12:593–598.

410 Rondeau, A., Peillon, S., Roynette, A., Sabroux, J.-C., Gelain, T., Gensdarmes, F., Rohde, V., Grisolia, C., and Chassefière, E. (2015). Char-  
411 acterization of dust particles produced in an all-tungsten wall tokamak and potentially mobilized by airflow. *Journal of Nuclear Materials*,  
412 463:873–876.

413 Rumpf, H. (1990). *Particle technology*. Chapman and Hall, London. OCLC: 472909018.

414 Salazar-Banda, G., Felicetti, M., Gonçalves, J., Coury, J., and Aguiar, M. (2007). Determination of the adhesion force between particles and a flat  
415 surface, using the centrifuge technique. *Powder Technology*, 173(2):107–117.

416 Stancu, C., Stokker-Cheregi, F., Moldovan, A., Dinescu, M., Grisolia, C., and Dinescu, G. (2017). Modification of W surfaces by exposure to  
417 hollow cathode plasmas. *Applied Physics A*, 123(10).

418 Szarek, T. R. and Dunn, P. F. (2007). An Apparatus to Determine the Pull-Off Force of a Conducting Microparticle from a Charged Surface. *Aerosol*  
419 *Science and Technology*, 41(1):43–50.

420 Takeuchi, M. (2006). Adhesion forces of charged particles. *Chemical Engineering Science*, 61(7):2279–2289.

421 Tolia, P. (2018). Lifshitz calculations of Hamaker constants for fusion relevant materials. *Fusion Engineering and Design*, 133:110–116.

422 Tolia, P., Riva, G., De Angeli, M., Ratynskaia, S., Daminelli, G., Lungu, C., and Porosnicu, C. (2018). Adhesive force distributions for tungsten  
423 dust deposited on bulk tungsten and beryllium-coated tungsten surfaces. *Nuclear Materials and Energy*, 15:55–63.

424 Wanka, S., Kappl, M., Wolkenhauer, M., and Butt, H.-J. (2013). Measuring Adhesion Forces in Powder Collectives by Inertial Detachment.  
425 *Langmuir*, 29(52):16075–16083.

426 Xie, H. (1997). The role of interparticle forces in the fluidization of fine particles. *Powder Technology*, 94(2):99–108.

427 Zafar, U., Hare, C., Hassanpour, A., and Ghadiri, M. (2014). Drop test: A new method to measure the particle adhesion force. *Powder Technology*,  
428 264:236–241.

429 Zhang, T., Peng, W., Shen, K., and Yu, S. (2015). AFM measurements of adhesive forces between carbonaceous particles and the substrates.  
430 *Nuclear Engineering and Design*, 293:87–96.